Sonochemically Produced Fluorocarbon Microspheres: A New Class of Magnetic Resonance Imaging Agent

Andrew G. Webb, PhD • Mike Wong, BS • Kenneth J. Kolbeck, BS • Richard L. Magin, PhD
Kenneth S. Suslick, PhD

With the intent of increasing the signal-to-noise ratio (SNR) of fluorine magnetic resonance imaging and enabling new applications, we have developed a novel class of agents based on protein encapsulation of fluorocarbons. Microspheres formed by high-intensity ultrasound have a gaussian size distribution with an average diameter of 2.5 μm. As with conventional emulsions, these microspheres target the reticuloendothelial system. However, our sonochemically produced microspheres, because of a high encapsulation efficiency, show increases in the SNR of up to 300% compared to commercially available emulsions. We also demonstrate an increase in the circulation lifetime of the microspheres within the bloodstream by more than 30-fold with a chemical modification of the outer surface of the microsphere. Finally, by encapsulating mixtures of fluorocarbons that undergo solid/liquid phase transitions, we can map temperature in the reticuloendothelial system, with signal changes of approximately 20-fold over a 5°C range.

Index terms: Magnetic resonance imaging • Perfluorocarbons • Sonochemistry • Temperature mapping • Microspheres

JMRI 1996; 6:675–683

Abbreviations: BSA = bovine serum albumin, DSC = differential scanning calorimetry, EPI = echo-planar imaging, FC-43 = oxypherol-containing perfluorotributylamine, FTPA = perfluorotripropylamine, LCBV = local cerebral blood volume, PEG = polyethylene glycol, PFOB = perfluorooctyl bromide, PTBA = perfluorotributylamine, PTBD = perfluoro-2,2,2',2'-tetramethyl-4,4'-bis(1,3-dioxalane), PTPA = perfluorotripropylamine, RES = reticuloendothelial system, RIF-1 = radiation-induced fibrosarcoma, SNR = signal-to-noise ratio, TEM = transmission electron micrograph, TNBS = trinitrobenzenesulphonic acid, U-FLARE = ultra-fast-low-angle-RARE.

From the Magnetic Resonance Engineering Laboratory, Department of Electrical and Computer Engineering (A.G.W., R.L.M.), and the School of Chemical Sciences (M.W., K.J.K., K.S.S.), University of Illinois at Urbana-Champaign, Urbana, Illinois. Presented at the 2nd annual meeting of the Society of Magnetic Resonance, San Francisco, 1994. Supported by the Whitaker Foundation, National Science Foundation Grant CHE-8915020, and National Institutes of Health Grant HL-25934. Magnetic resonance imaging experiments were carried out at the Biomedical Magnetic Resonance Laboratory at the University of Illinois, which is supported by the National Institutes of Health Research Resource Grant 1P1PR05964-01 and the Servants United Foundation. Received October 6, 1995; accepted March 25, 1996. **Address reprint requests to** A.G.W., Beckman Institute for Advanced Science and Technology, 405 North Mathews, Urbana, IL 60801.

THE INCREASING USE OF FLUORINE in magnetic resonance imaging is based on its high sensitivity, its lack of background signal in vivo, its low toxicity, and the ability to measure local oxygen pressure in tissues via changes in the fluorine spin-lattice relaxation time (T1). Fluorine MR has been used in a number of diverse areas of biomedical interest: the biodistribution of fluorinated anesthetics (1–3) and drugs (4–6); measurements of cerebral blood volume (7) and myocardial vascular volume (8); the distribution of fluorocarbons in the lung (9); applications in ophthalmology (10,11) and imaging the reticuloendothelial system (RES) (12–14); and measuring the spatially dependent cerebral and hepatic oxygen pressure (15–21) as well as the oxygen tension in tumors (21–27). A brief review of this literature is given below.

Chew et al (1) have shown that halothane, a gaseous anesthetic, was mainly localized in the lipophilic regions of the rabbit head, but they did not see fluorine signal arising from brain tissue. Wyrwicz and Conboy (2) used rotating frame experiments to investigate the nonuniform distribution of halothane within the brain, finding the highest concentration in the base of the brain. They also observed fluorine signal intensity in the brain up to 6.5 hours postanesthesia. Hashimoto et al (3) studied the biodistribution of enflurane, another anesthetic, in rats and obtained signal from the dorsal neck as well as mandibular adipose tissues. No definitive signal was observed from the brain, whereas a large signal intensity was recorded from the liver, intra-abdominal adipose tissue, and trunk adipose tissue. Arndt et al (4) investigated the bulk distribution of a trifluorinated neuroleptic (fluphenazine), spectroscopically detecting signal in vivo in the whole head, and ex vivo in the brain after excision. Nakada et al (5) showed that 2-fluoro-2-deoxy-D-glucose was taken up in the brain, spinal cord, and heart, whereas 3-fluoro-3-deoxy-D-glucose gave the highest signal intensity in the brain and ocular lens. The variation observed was attributed to different aldose reductase activity in the respective tissues. Maxwell et al (6) demonstrated that a fluorinated representative of a class of quinazoline antifolates (inhibitors of thymidylate synthase used in antibacterial and anticancer treatments) accumulated in the gallbladder, urinary bladder, and small intestine. Lu et al (7) used fluorine imaging to measure the local cerebral blood volume (LCBV) in cats as a function of the arterial pressure of CO_2. The authors

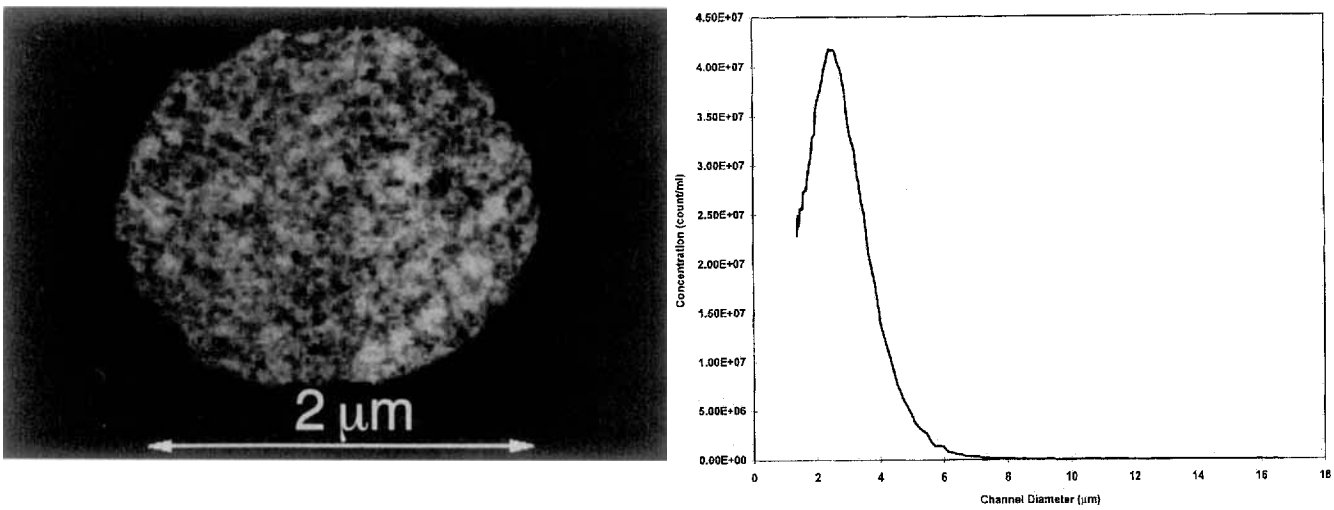

a. b.

Figure 1. (*a*) Transmission electron micrograph of a single perfluorononane-filled microsphere. The TEM preparation involves cross-linking with glutaraldehyde, staining with osmium tetroxide and potassium ferrohexacyanate, and embedding in a nonpolar medium. The sample is then ultramicrotomed to a thickness of 70 and imaged on a JEOL-100 TEM instrument. Staining techniques darken regions of high protein concentration. (*b*) Size distribution of sonochemically produced perfluorononane-filled microspheres. Particle size distribution was determined with an Elzone particle counter (model 180XY) and confirmed by light microscopy. Analysis showed that the purified n-C9F20 microspheres are present in concentrations of approximately 1.6×10^9 microspheres/ml with a Gaussian-like size distribution (mean diameter 2.5 microns, standard deviation 1.0 microns).

reported that the surface of the cortex has a high LCBV because of the large number of blood vessels found there. Thomas et al (9) showed that breathing of liquid perfluorocarbons could be used to image the lungs in mice, suggesting a viable method of gaining diagnostic information concerning pulmonary ventilation performance. Berkowitz et al (10,11) have applied fluorine imaging and spectroscopy to ophthalmology. Using surface coil localization and an inversion-recovery sequence with adiabatic pulses, they determined the intraocular pO_2 in vivo using perfluorotributylamine (PTBA).

Fluorine imaging of the RES is a natural application of fluorine MR because fluorocarbon emulsions are removed from the blood circulation by the liver and spleen. Ratner et al (12) and Freeman et al (13) used emulsified perfluorooctyl bromide (PFOB) and a driven equilibrium spin-echo imaging sequence to study the kinetics of the uptake of the perfluorinated emulsion in the liver and spleen: they also observed small signals from the lungs and salivary glands. The retention time of perfluorocarbons within the body was studied by Meyer et al (14), who established that the exponential half-lives for perfluorotripropylamine (PTPA) in the liver and spleen ranged from 100 to 190 days and the linear half-lives ranged from 175 to 300 days. The elimination pathway was determined to be primarily through exhalation via the lungs.

The measurement of the partial pressure of oxygen (pO_2) is made possible by the high solubility of oxygen in fluorocarbons as well as the reduction in the fluorine T1 value. The change in the relaxation parameter is caused by dipolar interactions between the paramagnetic oxygen molecule and the fluorine nuclei. This topic has been reviewed by Clark et al (15). Mason et al (16) measured the linear variation in T1 with oxygen for the perfluorocarbon emulsion oxypherol-ET (which contains PTBA). They used surface coil spectroscopy to determine that the pO_2 in a meth-A murine tumor in a mouse did not change significantly as the oxygen concentration of the breathing gas was increased to 95%. However, a large change in the pO_2 was observed in the liver. A similar calibration for fluosol-DA (PTBA) was carried out by Reid et al (17). Using the same fluorocarbon, Holland et al (18) used a novel chemical-shift-selective partial-saturation spin-echo imaging sequence for increased speed in determining the fluorine T1 and, hence, tissue oxygenation. Eidelberg et al (19) used PTBA to determine the cerebral intravascular pO_2 in cat brain. They found a fairly uniform distribution in the vascular structures but suggested a bimodal distribution in the cerebral cortex corresponding to arterial and venous capillary values. Fishman et al (20), using PTPA, showed that spleen and lung exhibit large increases in pO_2 in a rat when pure O_2 is breathed, whereas liver exhibits a much smaller rise. This observation was attributed to the low pO_2 in portal venous blood. Mason et al (21) have gone one step further in using oxypherol to measure both pO and temperature, establishing that the T1 of the CF3 and β-CF_2 in the fluorine spectrum depend on temperature and pO_2 to differing degrees.

Mapping oxygen tension in tumors is important in the area of radiotherapy. Oxygen-free radicals, formed by the interaction of ionizing radiation and molecular oxygen, are the toxic agents that destroy tumor cells. Solid tumors, which have a low concentration of oxygen, are particularly resistant to radiotherapy. Longmaid et al (22) showed that there was significant uptake of PTBA in the Walker sarcinoma in rats. Hees and Sotak (23) studied radiation-induced fibrosarcoma (RIF-1) tumors in C3H mice using trans-1,2-bis(perfluorobutyl)-ethylene. Oxygen levels in the tumor were found to be significantly enhanced after treatment with nicotinamide, a radiosensitizer, as compared to saline-treated controls. Fishman et al (24) used rats injected subcutaneously with mammary adenocarcinoma cells. After infusion with PTPA, the tumor oxygen level was unaffected by changing the inspired atmosphere from air to pure O_2. These results suggest that blood flow to this particular tumor is very low. Mason et al (25) studied the biodistribution of oxypherol and a mixture of perfluorodecalin and fluosol-DA. They found that less than 3% of the perfluorocarbons accumulated in the meth-A tumors in Balb/C mice but concentrated instead within the spleen and liver.

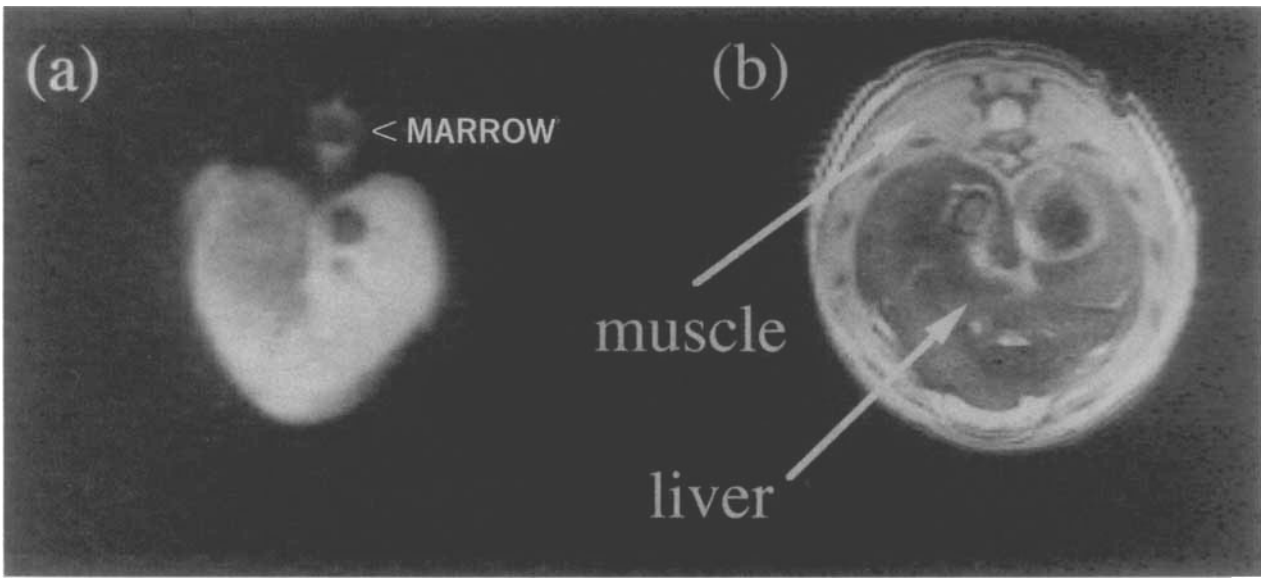

Figure 2. Comparison of fluorine (*a*) and proton (*b*) images through the abdominal region of the rat, acquired with a double-tuned Alderman-Grant RF coil without any repositioning. The arrows indicate the liver and bone marrow in which the microspheres accumulated. The image is viewed from the tail of the rat.

Most perfluorocarbon emulsions used in the studies described above have the disadvantage of multiple chemical shifts and short values of the spin-spin relaxation time (T2). Sotak et al (26) proposed the use of perfluoro-2,2,2',2'-tetramethyl-4,4'-bis(1,3-dioxalane) (PTBD) as a partial solution to these limitations. Two-thirds of the fluorine molecules resonate at a single frequency, these CF3 groups have relatively long T2 values, and homonuclear fluorine-fluorine scalar coupling is essentially absent. Dardzinski and Sotak (27) have also used perfluoro-15-crown-5-ether, which contains a single peak from the 20 chemically equivalent fluorine atoms. The T2 value is long, and there is no scalar coupling. The authors used inversion-recovery echo-planar imaging (EPI) to measure tissue oxygenation in mice with RIF-1 tumors using this compound.

A number of imaging techniques have been developed to increase the low sensitivity of fluorine imaging. Barker et al (28) have used EPI and Bornet et al (29) have used fast imaging using the ultra-fast-low-angle-RARE (U-FLARE) technique and Freeman et al (13) and Ratner et al (12) employed a driven equilibrium spin-echo sequence. In each of these studies, the total data acquisition time was reduced substantially compared with a standard spin-echo imaging sequence, but no quantitative comparison between the techniques has been established. It should be noted that the multiple chemical shifts present in most perfluorocarbon spectra present two problems for imaging. The first is a misselection when a slice-selection gradient is applied in the imaging sequence. Ozdemirel and Nalcioglu (30) and Lee et al (31) have combined multislice imaging, where the misselection artifact was matched to the desired slice gap with the Dixon technique to overcome this effect. The second is the chemical shift artifact that is manifest during the readout gradient in the imaging sequence. Busse et al (32) have used two postprocessing techniques (noise-masked deconvolution and maximum entropy deconvolution) to remove the chemical shift artifacts from images using cis/transperfluorodecalin and PTBA. They reported that the processed images had a similar or enhanced signal-to-noise ratio (SNR) to the unprocessed images.

Almost all of the in vivo studies have used fluorocarbon or perfluorocarbon emulsions, which are simply dispersions of micron-sized fluorocarbon droplets stabilized in an aqueous environment. Although emulsions have been proven to be effective and safe, there is little or no possibility to alter their biodistribution characteristics through chemical modification. A second general problem exists, in that many commercial emulsions only contain 10% to 40% weight per volume (w/v) of the active fluorocarbon. The low effective dose means that multiple injections are often necessary or that the SNR for fluorine imaging is insufficient to measure pO_2 or temperature.

In this study, we consider an alternative approach: the use of sonochemically produced protein microspheres (33) filled with a fluorocarbon liquid. Similar air-filled microspheres are currently in clinical trials as contrast agents in ultrasound imaging (34–37). This paper presents initial results of in vitro and in vivo studies of microspheres using bovine serum albumin (BSA) as the protein shell and containing a fluorocarbon. A single compound, perfluorononane ($n\text{-}C_9F_{20}$), is used in fluorine imaging, whereas a mixture of fluorocarbons and hydrocarbons is used for temperature mapping. As conventional fluorocarbon emulsions, the microspheres target the RES and give rise to high SNR fluorine images. Clearance studies show that the half-life of the agent is comparable to emulsions. However, the new formulation offers several advantages. First, because the encapsulation process is extremely efficient, the volume of the fluorocarbon that can be delivered per unit injection volume is up to six times greater than for typical emulsion preparations, increasing signal intensity and/or decreasing data acquisition time. Second, the surface reactive groups of the microspheres' shell can be modified chemically to control the lifetime of the spheres within the bloodstream. Third, the encapsulation process allows a mixture of compounds of exact formulation to be delivered to the RES. This final property has enabled us to carry out temperature mapping via changes in the magnetic resonance signal caused by solid/liquid phase transitions.

It should be noted that standard polymeric microspheres and chemically cross-linked protein micro-

a. b.

Figure 3. (*a*) Transverse fluorine projection images at various time points after injection of the microcapsules. The liver is seen clearly with a small signal from the bone marrow. The images are scaled to the same noise level. Spin-echo imaging sequence parameters are in the main text. (*b*) Corresponding coronal fluorine projection images, showing accumulation of the microspheres within the spleen, posterior to the liver, as well as the liver itself. Imaging parameters are as for the transverse images.

spheres (using, for example, glutaraldehyde) have a potential disadvantage when compared to sonochemically produced microspheres, namely the induction of an immune response. Studies using albunex (a sonochemically produced, air-filled albumin microsphere) have shown that no immune response is produced in humans (38). Perfluorocarbons themselves have a long history of being used as blood substitutes because of their inertness and high oxygen-carrying capability.

• MATERIALS AND METHODS

Generation of Microcapsules

Ultrasound irradiation at the interface of an aqueous protein solution and a nonpolar liquid has been shown to produce proteinaceous microspheres at high concentrations with narrow size distributions (33,34). The formation of these spheres involves both emulsification and a chemical cross-linking of protein molecules. The protein forms a thin shell surrounding the encapsulated nonpolar liquid. The cross-linking reaction principally involves disulfide bond formation by sonochemically produced superoxide-free radicals. These radicals arise from the sonolysis of water during acoustic cavitation (39). The n-C_9F_{20} microspheres are very stable, showing minimal degradation (<10%) after storage in .1-M Hepes buffer, pH 7.4, over 6 months at 4°C. Microencapulation of n-C_9F_{20} was carried out using high-intensity ultrasound irradiation of a 1:2 (*v*/*v*) mixture of n-C_9F_{20} with 5% (*w*/*v*) aqueous BSA solution. The BSA solution was layered over the n-C_9F_{20} at an initial temperature of 23°C and pH 7.0. With a titanium acoustic horn (diameter 1.3 cm) positioned at the organic-aqueous interface, the mixture was irradiated (Heat Systems XL2020, Farmingdale, NY) for 3 minutes at an acoustic power of approximately 150 W/cm^2. The microspheres remained as a suspension in the native protein solution. To separate the microspheres from the nonreacted protein, a centrifuge filter with a molecular weight cutoff of 100 kD was used (native BSA has a molecular weight of 66.5 kD). Centrifugation was performed at 5,000 G for 5 minutes, and the microspheres were then resuspended in buffer. This process was repeated five times. Particle size distribution was determined with an Elzone particle counter (model 180XY, Elmhurst, IL) and confirmed by light microscopy. Analysis showed that the purified n-C_9F_{20} microspheres are present in concentrations of approximately 1.6×10^9 microspheres/ml with a gaussian-like size distribution (mean diameter 2.5 μm, standard deviation 1.0 μm). Transmission electron micrographs (TEM) of a single microcapsule were obtained (Fig. 1a). The TEM preparation involves cross-linking with glutaraldehyde, staining with osmium tetroxide and potassium ferrohexacyanate, and embedding in a nonpolar medium. The sample is then ultramicrotomed to a thickness of 70nm and imaged on a JEOL-100 TEM instrument. Staining techniques darken regions of high protein concentration. Figure 1b shows the size distribution achieved: diameters below 1 μm cannot be measured using the present experimental apparatus. Immediately before injection into rats, a final filtration step is performed using a .45-μm centrifuge filter (Millipore, St. Louis, MO). Any denatured protein, native protein, and unencapsulated fluorocarbon pass through the filter and are separated from the microspheres.

Magnetic Resonance Imaging

All magnetic resonance imaging experiments were carried out at a magnetic field strength of 4.7 T, using a 22-cm clear-bore horizontal superconducting magnet. Pulse programming and data acquisition were performed using a SISCO VIS imager/spectrometer (Spectroscopy Imaging Systems Corporation, Palo Alto, CA). For phantom studies, a two-turn solenoidal coil was used for transmission and reception. For imaging of the RES of rats, an Alderman-Grant coil (4 cm in diameter) was constructed (40), which could be tuned to 200 MHz for protons and 188 MHz for fluorine. Anesthesia of the animals was induced by metofane, followed by intramuscular injection of .1 ml/100 g body weight of ketamine/acepromazine (10:1 *v*/*v*).

Two-dimensional fluorine projection images, ie, no slice selection, were obtained using a spin-echo imaging sequence, a field of view of 6 × 6 cm, an echo time of 20 ms, with a recycle delay of 2 s. Four signal averages were acquired using a data matrix size of 128 × 64, zero-filled to 128 × 128, and the total imaging time was 8.5 minutes per image. Proton images were acquired using identical data acquisition parameters on a 2-mm-thick slice. For

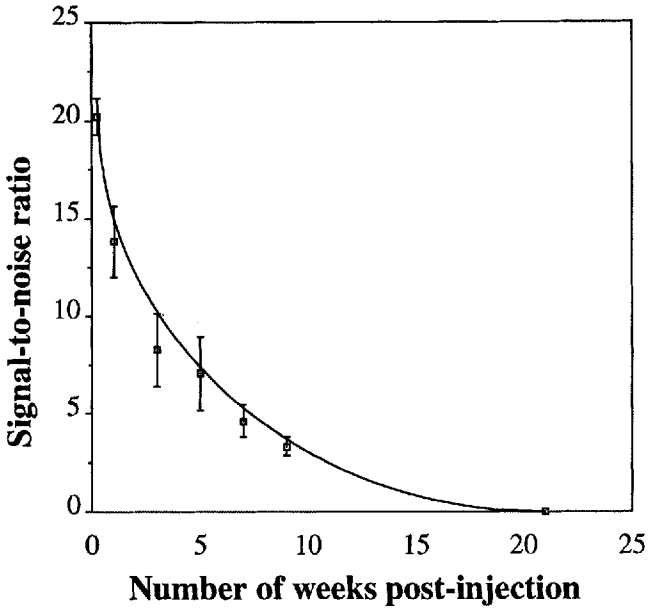

Figure 4. Fluorine SNR as a function of time postinjection, averaged over the whole liver, of the images presented in Figure 3. Each data point represents the mean of three animals, with error bars indicating one standard deviation above and below the mean. The elimination half-life was calculated to be 35 +/− 4 days.

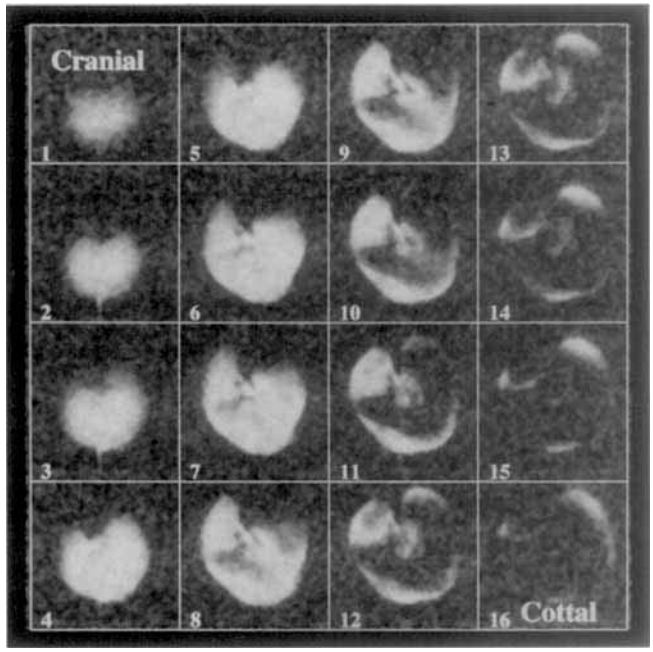

Figure 5. Three-dimensional fluorine imaging using 16 phase-encoding steps in the third dimension. The 128 × 64 × 16 data matrix was zero-filled to 128 × 128 × 16: total data acquisition time was approximately 16 minutes.

three-dimensional fluorine imaging, 16 phase-encoding steps were taken in the second encoding direction using a field of view of 2.4 cm. One signal average was acquired with a relaxation delay of 1 second, for a total data acquisition time of 16 minutes.

Chemical Modification of the Protein Shell

The outer surface protein shell of the microsphere contains a number of chemically active moieties. The primary amine groups from the sidechains of the amino acid lysine offer the opportunity of attaching polyethylene glycol (PEG) to the outer surface of the microspheres. The polymer inhibits phagocytosis of particulate matter by the RES and increases the blood circulation time of the microspheres.

After microencapsulation of the n-C_9F_{20}, PEG was attached using the procedure of Abuchowski et al (41). With a threefold excess of monomethoxy PEG 2000 polymer (Aldrich, Milwaukee, WI; 8.0 g, 3.75 mmol), the terminal hydroxyl group of the glycol is coupled via an intermediate formed with cyanuric chloride to the primary amine groups of the protein. The microspheres were suspended in an aqueous solution of sodium tetraborate (Aldrich; 50 ml, .1 M). After cooling to 4°C, the activated PEG-2000 was added and the solution was stirred for 10 to 12 hours. Unreacted PEG was removed through dialysis with a 300-kD molecular weight cutoff membrane (Spectrum, Los Angeles, CA). HEPES buffer was used as the dialyzing solution (Sigmo, St. Louis, MO; .1M, pH 7.4). Dialysis continued for 3 days with a change in the dialyzing solution every 12 hours. The covalent attachment of PEG was confirmed by absorbance measurements at 340 nm from 2,4,6-trinitrobenzenesulphonic acid (TNBS) (42). This compound reacts with primary amine groups. Any group on the protein surface that has not been conjugated by PEG will therefore react with the TNBS. This method of increasing the lifetime of particles within the bloodstream has been used in previous studies using liposomes and other particulate agents (43).

• RESULTS

Determination of Capture Rate, Biodistribution, and In Vivo Half-Life

The first experiment measured the capture rate of the microspheres. Equal volumes (1 ml) of neat n-C_9F_{20} and encapsulated microspheres were separately placed in a two-turn solenoidal coil within the magnet. SNR measurements were made using a single 90° excitation pulse and the statistics of 10 experiments were computed. The average signal intensity from the microspheres was calculated to be 70% of the neat liquid, equivalent to a w/v value of approximately 140% and v/v of 70%. Previous fluorine imaging of commercial preparations of emulsions include oxypherol-containing perfluorotributylamine (FC-43) at 25% w/v (23), fluosol-DA, a mixture containing 14.5% w/v perfluorodecalin and 6% perfluorotripropylamine (FTPA) (15), perfluorooctylbromide (PFOB) at 100% w/v, perfluoro-15-crown-5-ether at 40% v/v (14), and FTPA emulsified in egg yolk lecithin and Tyrode's buffer at 40% w/v (17). It should be noted that many of these preparations are used in blood substitiute studies and are not optimized for fluorine imaging. Because this microencapsulation process can be applied potentially to any nonpolar liquid, it should provide a significant increase in the sensitivity of fluorine imaging of any number of different fluorocarbons.

To study the biodistribution and clearance time of n-C_9F_{20}-filled microspheres, magnetic resonance imaging studies were performed on 21 rats (Fischer 344, female, 150–200 g). These animals were injected via the tail vein with 10 ml of the microsphere suspension per kilogram of body weight, corresponding to a dose of 1.3 g n-C_9F_{20}/kg. The biodistribution of the microspheres can be seen by comparing fluorine and proton images of the same animal as shown in Figure 2. High intensity is seen in the liver, as expected, with no signal from the muscle, although there is evidence of minor uptake in the bone marrow, as expected. Within the liver, the signal intensity

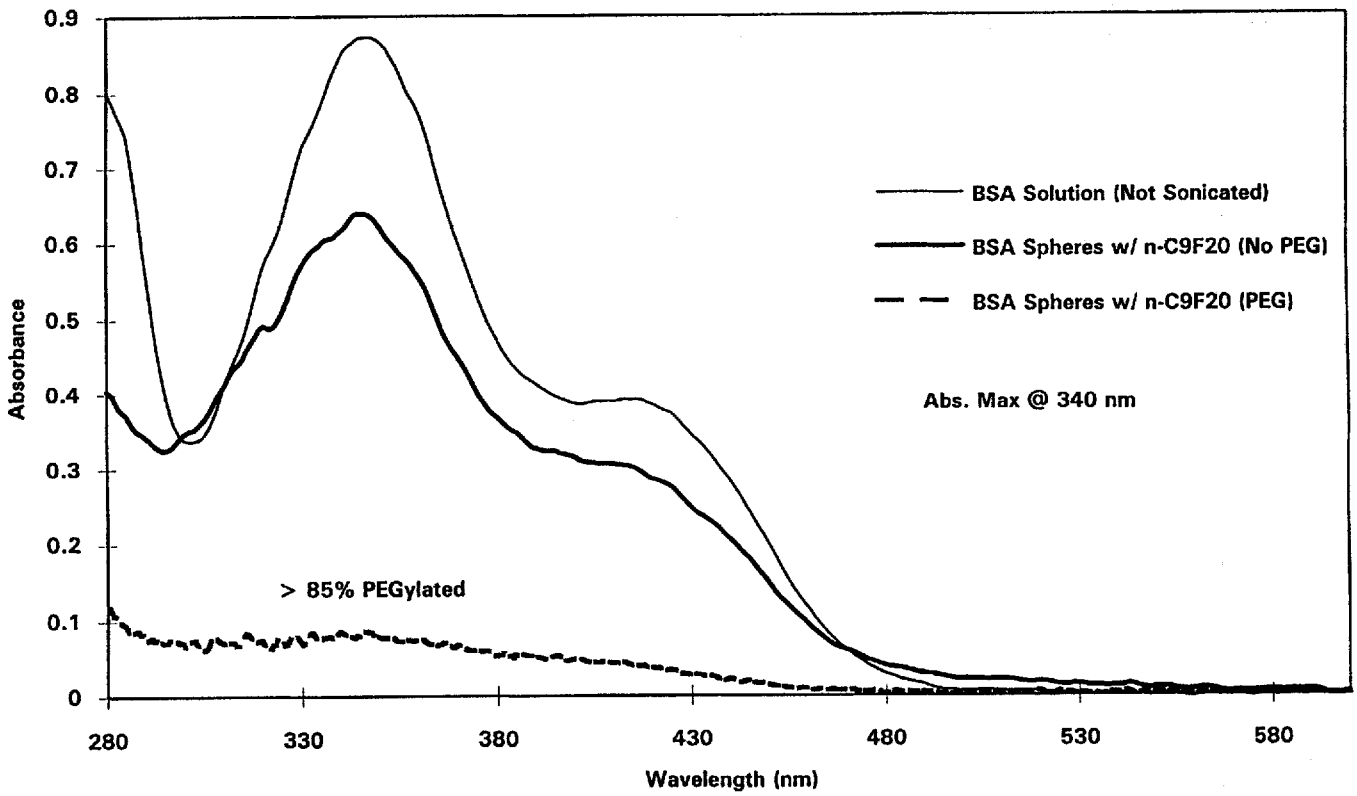

Figure 6. Reaction of BSA native solution, BSA n-C9F20 microspheres without a PEG coating and BSA n-C9F20 microspheres with PEG covalently attached, in the presence of 2,4,6-trinitrobenzenesulphonic acid. This reacts with any primary amine groups that have not been conjugated by PEG, producing an absorption maximum at 340 nm. The n-C9F20 PEG-coated microspheres showed greater than 85% reduction in the free primary amine groups at the protein surface.

is not uniform because the projection image contains signal from all of the various lobes of the liver and also signal from the spleen, which typically lies on one side of the animal. Although the fluorine spectrum of n-C_9F_{20} shows three distinct groups of peaks, widely separated in the chemical shift domain, selective radiofrequency excitation was used to ensure that the only fluorine nuclei contributing to the final image are those of the CF3 groups. Any chemical shift artifacts in the image are therefore eliminated.

To determine the retention time of the perfluorocarbon within the RES, 21 animals were assigned to seven separate groups of three animals each. The animals were imaged and then killed at 4 hours, 1 day, and 3, 5, 7, 9, and 21 weeks after injection of the microspheres. Figure 3a shows representative transverse images obtained for one of the rats in each group. The decrease in signal intensity as a function of time postinjection is clear. Once again, the signal intensity is not uniform. Because each image corresponds to a different animal, it seems reasonable that the differences are caused by the particular orientation of the lobes of the liver and the spleen. Figure 3b shows corresponding coronal images in which the spleen can be identified below the liver. The SNR was computed for each transverse image using an average signal intensity over the whole liver. The mean of the ratios was computed for the three rats in each group, and the results are shown in Figure 4, with error bars representing one standard deviation above and below the mean. The values indicate an approximate half-life of n-C_9F_{20} of 35 +/− 4 days, which is comparable to a number of the fluorocarbon emulsions. It should be emphasized that this is not a measurement of the half-life of the microspheres themselves. Low pH has been shown to destroy the microspheres in vitro; thus, the acidic environment within the digestive organelles of the macrophages probably ruptures and digests the protein shell. The n-C_9F_{20} is then most likely excreted through the lungs via expiration, as has been documented for many other fluorocarbon emulsions (24–26). No long-term physiologic effects were seen during the period of the experiment and weight gain was normal. Three-dimensional imaging of the RES was also performed using the same RF coil. Imaging parameters are reported under

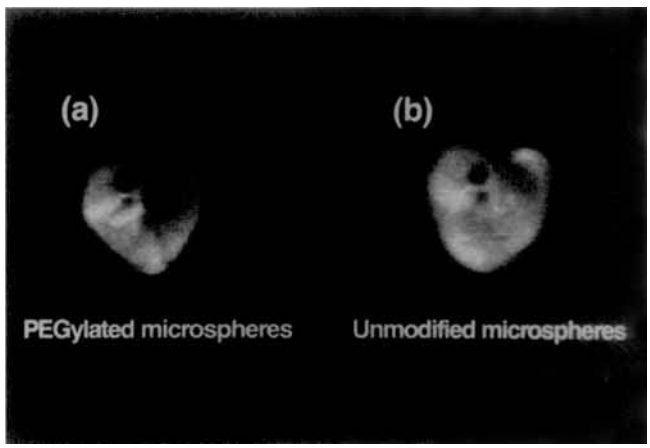

Figure 7. Transverse in vivo fluorine projection image of rats 2 days after injection of (*a*) PEGylated and (*b*) nonPEGylated microspheres. The signal intensities are the same in both cases, showing that PEGylation does not effect the efficacy of RES fluorine imaging while offering the advantage of controlling the lifetime of the microspheres in the bloodstream.

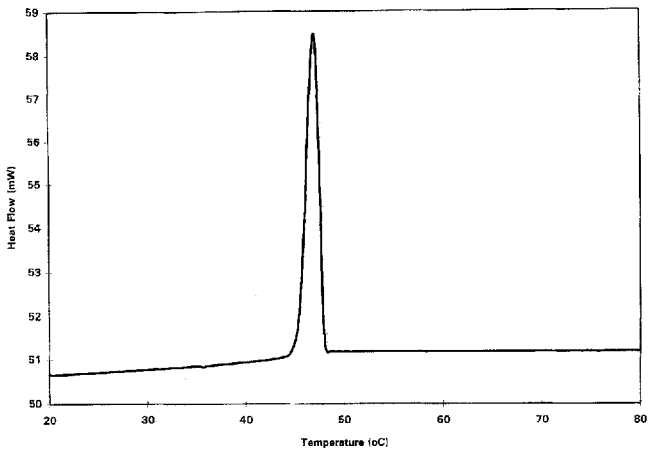

Figure 8. DSC of phase-transition agent, consisting of 2-trifluoromethyl benzamide and methyl laurate in a molar ratio of 5.2:1. The results show a reasonably sharp transition over the temperature range of 42 to 44°C.

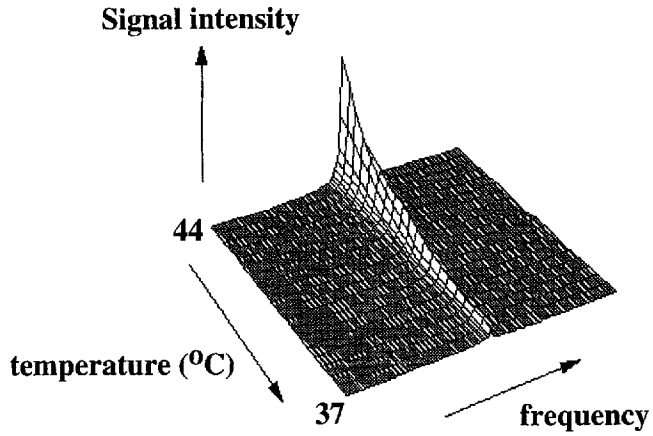

Figure 9. SNR as a function of temperature for 2-trifluoromethyl benzamide and methyl laurate in a molar ratio of 5.2:1. There is a 20-fold change in signal intensity over a 5°C temperature range.

Materials and Methods. These images are shown in Figure 5, in which the full nonuniformity of the signal rom the various liver lobes, previously alluded to, can be seen.

Effect of Chemical Modification

Figure 6 shows the absorbance of nonPEGylated and PEGylated microspheres: the absorbance spectra indicate that more than 85% of the amine groups on the surface of the BSA shell have reacted with PEG. The extent of chemical modification can be easily controlled stoichiometrically. The blood circulation time of the PEGylated microspheres was measured in vivo by obtaining blood samples at regular intervals via cannulation of the external jugular vein and measuring the n-C_9F_{20} content from the fluorine NMR signal intensity. Anesthesia was induced using ketamine/acepromazine as described earlier. Three animals were injected with nonPEGylated and three were injected with PEGylated microspheres (identical doses 1.3 g n-C_9F_{20}/kg). After injection, 100 μl of blood was removed at appropriate time points and stored in heparinized saline. The circulation half-lives of microspheres with and without PEG attachment were 70 minutes and 2.5 minutes, respectively. The unmodified microspheres are removed almost immediately from the blood by the RES, while the modified microspheres remained in the circulation almost 30 times longer. Imaging studies were also performed to investigate whether the chemical modification altered the biodistribution of the microspheres and whether the NMR signal intensity of the encapsulated perfluorocarbon was altered. Transverse projection images of four rats (Sprague-Dawley, female, 250 g) injected with equal doses (1.3 g n-C_9F_{20}/kg) of PEGylated and nonPEGylated microspheres were taken 2 days after injection of the agent using data-acquisition parameters described previously. Representative images are shown in Figure 7, showing accumulation of both forms of microspheres within the RES. The fluorine NMR signal intensity from each was the same within experimental error.

Encapsulation of Fluorocarbon Mixtures for Temperature Mapping

A number of proton MRI techniques have been developed to map temperature; the relevant parameters are the chemical shift of the water peak (44,44a), the proton T1 relaxation time (45–48), the total water magnetization (49), and the diffusion coefficient of the water protons in tissue (50–52). Liposome-encapsulated cobalt complexes also have been shown to be effective in vivo (53,53a). The main advantages of the MRI technique are its noninvasive character, the high spatial and temporal resolution attainable, and that whole-body temperature analysis is feasible, unlike microwave and infrared techniques, which are limited to surface characterizations caused by the limited tissue penetration of these electromagnetic techniques. Using such MRI methods, the field of mapping temperature in vivo has shown a recent rapid expansion. The proton-based methods of mapping temperature are particularly suited to studies of muscle and other relatively stationary organs. The RES, in particular, presents problems because of motion artifacts and local changes in magnetic susceptibility due to respiration. An alternative approach to temperature measurement is to use the magnetic resonance properties of compounds undergoing a phase transition. One such method investigated the in vitro change in proton relaxation times of liquid crystals arising from smectic to nematic phase changes (54). This study concluded that the technique was impractical for in vivo studies because of the small changes in proton signal intensity being masked by the large background signal.

Our new approach uses the magnetic resonance properties of solid/liquid phase transitions. Signal intensity is present when a compound is in the liquid phase and absent when it becomes solid. The key problem thus far has been the lack of a single fluorocarbon compound, which combines high NMR signal intensity with a phase-transition temperature in a range relevant to, for example, hyperthermia studies. We have developed a mixture of compounds that has these desirable properties. The sonochemical encapsulation of a fluorocarbon-hydrocarbon mixture, designed to melt at a specific temperature range, can be prepared and targeted to the RES. Two such formulations have been investigated for use in the temperature range of 35 to 45°C. First, 2-trifluoromethyl benzamide (PCR, Gainesville FL; melting point 161-162°C) and methyl laurate (Sigma Chemicals; melting point 4.3°C) were combined in a molar ratio of 5.2:1. 2-Trifluoromethyl benzamide has three equivalent fluorines that give rise to a single NMR peak and is commercially available. Methyl laurate serves to colligatively depress the melting point of the fluorocarbon. Differential scanning calorimetry (DSC) studies were carried out to determine the melting point range of the formulation when

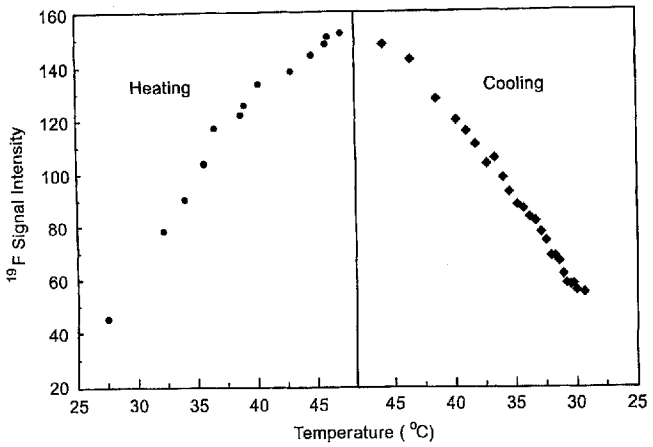

Figure 10. Change in SNR as a function of temperature for the a mixture of poly(chlorotrifluoroethylene) (2 g) and n-C9F20 (.15 ml) in excised rat liver. The liver was heated with a surface contact microwave diathermy applicator. A reversible signal increase on heating and decrease on cooling is seen.

encapsulated. The results are shown in Figure 8, displaying a transition at 42 to 44°C as desired. In vitro imaging experiments have been carried out to test the dependence of the MRI signal intensity on temperature; 1 ml of the encapsulated mixture was heated to 44°C and allowed to cool in the magnet. Fluorine spectra were acquired every 10 seconds, using a single signal average, and correlated with temperature measurements from a fiber optic probe (Luxtron, Mountain View, CA, model 755) inserted into the sample. Figure 9 shows the decrease in signal intensity in transition from the liquid to the solid phase, corresponding to a 20-fold decrease in signal intensity over a 5° temperature range.

A second mixture used consisted of poly(chlorotrifluoroethylene) (2 g, mp 58–60°C, Halocarbon) and n-C_9F_{20} (.15 ml, bp 125-126°C), which were combined to give a mixture that melted in the range 45 to 50°C. Once encapsulated in the microspheres, this fluorocarbon mixture was injected into the rat via the tail vein at a dose of 1 ml/100 g. After 30 minutes, the rat was sacrificed and the liver was excised. The liver was then heated with a 15-mm-diameter ceramic-filled surface contact microwave diathermy applicator (2.45 GHz, power rating 15W, Elmed Corporation, Addison, IL). The change in the fluorine NMR signal intensity was monitored upon heating and subsequent cooling. As the core of the microsphere melts, the fluorine linewidth narrows and a substantial increase in SNR was observed. Figure 10 shows the fluorine signal intensity plotted as a function of temperature, showing a reversible phase-transition upon heating and subsequent cooling. Data acquisition parameters and RF coils were as described for the previous heating experiment.

• CONCLUSION

The data presented in this paper show that protein microencapsulation of perfluorocarbons results in a new imaging agent that targets the RES and provides high-quality fluorine images in a reasonable data acquisition time. Compared with commercially available emulsions, the attainable SNR is up to three times larger, based on a high encapsulation efficiency, and this method can be used for any fluorocarbon. The sonochemically produced microspheres have BSA as the shell structure, which can easily be chemically modified: attachment to polyethylene glycol was shown to significantly increase the blood lifetime by more than a factor of 30.

Because the microcapsules can be formed using any nonpolar liquid, these particles offer a new method for entrapping and delivering MR imaging agents that consist of single compounds or mixtures of more than one chemical species. Using a suitable combination of different fluorocarbons, such that the solid/liquid phase transition temperature of the mixture lies within physiologic limits, local temperature changes can be monitored noninvasively.

Acknowledgments: The authors thank Laura Burger for assistance in the external jugular vein cannulation and Lisa Wilmes for assistance in microwave heating.

References

1. Chew WM, Moseley ME, Mills PA, et al. Spin-echo fluorine magnetic resonance imaging at 2T: in vivo spatial distribution of halothane in the rabbit head. Magn Reson Imaging 1987; 5: 51–56.
2. Wyrwicz AM, Conboy CB. Determination of halothane distribution in the rat head using 19F NMR techniques. Magn Reson Med 1989; 9:219–228.
3. Hashimoto T, Ikehira H, Fukuda H, Ueshima Y, Tateno Y. Study of biodistribution of enflurane in rats with in-vivo 19F MRI. Magn Reson Imaging 1991; 9:577–581.
4. Arndt DC, Ratner AV, Fauli K, Barchas JD, Young SW. 19F magnetic resonance imaging and spectroscopy of a fluorinated neuroleptic ligand: in-vivo and in-vitro studies. Psychol Res 1988; 25:73–79.
5. Nakada T, Kwee IL, Card PJ, Matwoyoff NA, Griffey BV, Griffey RH. Fluorine-19 NMR imaging of glucose metabolism. Magn Reson Med 1988; 6:307–313.
6. Maxwell RJ, Frenkiel TA, Newell DR, Bauer C, Griffiths JR. 19F nuclear magnetic resonance imaging of drug distribution in-vivo: the disposition of an antifolate anticancer drug in mice. Magn Reson Med 1991; 17:189–196.
7. Lu D, Joseph PM, Greenberg JH, Lin R, Mukherji B, Sloviter HA. Use of 19F magnetic resonance imaging to measure local cerebral blood volume. Magn Reson Med 1993; 29:179–187.
8. Joseph PM, Fishman JE, Mukherji B, Sloviter HA. In-vivo 19F imaging of the cardiovascular system. J Comput Assist Tomogr 1985; 9(6):1012–1019.
9. Thomas SR, Clark LC, Ackerman JL, et al. MR imaging of the xlung using liquid perfluorocarbons. J Comput Assist Tomogr 1986; 10:1–9.
10. Berkowitz BA, Wilson CA, Hatchell DL, London RE. Quantitative determination of the partial oxygen pressure in the vitrectomized rabbit eye in-vivo using 19F NMR. Magn Reson Med 1991; 21: 233–241.
11. Berkowitz BA, Wilson CA, Hatchell DL. Oxygen kinetics in the vitreous substitute perfluorotributylamine: a 19-F NMR study in-vivo. Invest Opthalmol Vis Sci 1991; 32:2382–2387.
12. Ratner AV, Hurd R, Muller HH, et al. 19F magnetic resonance imaging of the reticuloendothelial system. Magn Reson Med 1987; 5:548–554.
13. Freeman DM, Muller HH, Hurd RE, Young SW. Rapid 19F magnetic resonance imaging of perfluorooctyl bromide in vivo. Magn Reson Imaging 1988; 8:61–64.
14. Meyer KL, Carvlin MJ, Mukherji B, Sloviter HA, Joseph PM. Fluorinated blood substitute retention in the rat measured by fluorine-19 magnetic resonance imaging. Invest Radiol 1992; 27:620–627.
15. Clark LC, Ackerman JL, Thomas SR, et al. Perfluorinated organic liquids and emulsions as biocompatible NMR imaging agents for 19F and dissolved oxygen. Adv Exp Med Biol 1984; 180:835–845.
16. Mason RP, Nunnally RL, Antich PP. Tissue oxygenation: a novel determination using 19F surface coil spectroscopy of sequestered perfluorocarbon emulsion. Magn Reson Med 1991; 18:71–79.
17. Reid RS, Koch CJ, Castro ME, et al. The influence of oxygenation on the 19F spin-lattice relaxation rates of fluosol-DA. Phys Med Biol 1985; 30:677–686.
18. Holland SK, Kennan RP, Schaub MM, D'Angelo MJ, Gore JC. Imaging oxygen tension in liver and spleen by 19F NMR. Magn Reson Med 1993; 29:446–458.
19. Eidelberg D, Johnson G, Barnes D, et al. 19F NMR imaging of blood oxygenation in the brain. Magn Reson Med 1988; 8: 344–352.

20. Fishman JE, Joseph PM, Carvlim MJ, Saadi-Elmandjra M, Mukherji B, Sloviter HA. Oxygen sensitive 19-F NMR imaging of the vascular system in-vivo. Magn Reson Imaging 1987; 5: 279–285.
21. Mason RP, Shukla H, Antich PP. In-vivo oxygen tension and temperature: simultaneous determination using 19F NMR spectroscopy of perfluorocarbon. Magn Reson Med 1993; 29: 296–302.
22. Longmaid HE, Adams DF, Neirinckx RD, et al. In vivo 19F imaging of liver tumor and abscess in rats: preliminary results. Invest Radiol 1985; 20:141–145.
23. Hees PS, Sotak CH. Assessment of changes in murine tumor oxygenation in response to nicotinamide using 19F NMR relaxometry of a perfluorocarbon emulsion. Magn Reson Med 1993; 29:303–310.
24. Fishman JE, Joseph PM, Floyd TF, et al. In-vivo measurements of vascular oxygen tension in tumors using MRI of a fluorinated blood substitute. Magn Reson Imaging 1987; 5: 279–285.
25. Mason RP, Antich PP, Babcock EE, Gerberich JL, Nunnally RL. Perfluorocarbon imaging in-vivo: an 19F MRI study in tumor-bearing mice. Magn Reson Imaging 1989; 7:475–485.
26. Sotak CH, Hees PS, Huang H-N, Hung MH, Krespan CG, Raynolds S. A new fluorocarbon for use in fluorine-19 magnetic resonance imaging and spectroscopy. Magn Reson Med 1993; 29:188–195.
27. Dardzinski BJ, Sotak CH. Rapid tissue oxygen tension mapping using 19F inverson-recovery echo-planar imaging of perfluoro-15-crown-5-ether. Magn Reson Med 1994; 32:88–97.
28. Barker BR, Mason RP, Peshock RM. Echo planar imaging of perfluorocarbons. Magn Reson Imaging 1993; 11:1165–1172.
29. Bornet P, Norris DG, Koch H, Dreher W, Reichelt H, Leibfritz D. Fast perfluorocarbon imaging using 19F-UFLARE. Magn Reson Med 1993; 29:226–234.
30. Ozdemirel B, Nalcioglu O. Correction of chemical-shift artifacts in multislice F-19 imaging with perfluorooctyl bromide. Magn Reson Med 1992; 23:324–332.
31. Lee HK, Nalcioglu O, Buxton RB. Correction for chemical-shift artifacts in 19F imaging of simultaneous multislice imaging. Magn Reson Med 1991; 21:21–29.
32. Busse LJ, Pratt RG, Thomas SR. Deconvolution of chemical shift spectra in two- or three-dimensional 19F MR imaging. J Comput Assist Tomogr 1988; 12:824–835.
33. Suslick KS, Grinstaff MW. Protein microencapsulation of nonaqueous liquids. J Am Chem Soc 1990; 112:7807–7809.
34. Suslick KS, Grinstaff MW. Air-filled proteinaceous microbubbles: synthesis of an echo contrast agent. Proc Natl Acad Sci U S A 1991; 88:7708–7710.
35. Feinstein SB. Contrast echocardiography. Clin Cardiol 1991; 14:V1–V3.
36. Keller MW, Glasheen W, Kaul S. Albunex: a safe and effective commercially produced agent for myocardial contrast echocardiography. J Am Soc Echocardiogr 1989; 2:48–54.
37. Suslick KS. Sonochemistry. Science 1990; 247:1439–1445.
38. Christiansen C, Vebner AJ, Muan B, et al. Lack of an immune response to Albunex: a new ultrasound contrast agent based on air-filled albumin microspheres. Int Arch Allergy Immunol 1994; 104:372–378.
39. Suslick KS, Goodale JW, Wang HH, Schubert PF. Sonochemistry and sonocatalysis of metal carbonyls. J Am Chem Soc 1983; 105:5781–5783.
40. Alderman DW, Grant DM. An efficient decoupler coil design which reduces heating in conductive samples in superconducting spectrometers. J Magn Reson 1979; 36:447–451.
41. Abuchowski A, Es TV, Palczuk NC, Davis FF. Alteration of immunological properties of bovine serum albumin by covalent attachment of polyethylene glycol. J Biol Chem 1977; 252: 3578–3581.
42. Habeeb AFSA. Determination of free amino groups in proteins by trinitrobenzenesulfonic acid. Anal Biochem 1966; 14: 328–332.
43. Maruyama K, Yuda T, Okamoto A, Kojima S, Suginaka A, Iwatsuru M. Prolonged circulation time in vivo of large unilamellar liposomes composed of distearoyl phosphatidylcholine and cholsterol containing amphipathic poly(ethylene glycol). Biochim Biophys Acta 1992; 1128:44–49.
44. De Poorter J, De Wagter C, De Deene Y, Thomsen C, Stahlberg F, Achten E. The proton-reference frequency-shift method compared with molecular diffusion for quantitative measurement of two-dimensional time-dependent temperature distribution in a phantom. J Magn Reson, Series B 1994; 103:234–241.
44a. De Poorter J, De Wagter C, De Deene Y, Thomsen C, Stahlberg F, Achten E. Noninvasive MRI thermometry with the proton resonance frequency (PRF) method: in vivo results in human muscle. Magn Reson Med 1995; 33:74–81.
45. Parker DL. Applications of NMR imaging in hyperthermia: an evaluation of the potential for localized tissue heating and noninvasive temperature monitoring. IEEE Trans Biomed Eng 1984; 31:161–167.
46. Young IR, Hand JW, Oatridge A, Prior MV, Forse GR. Further observations on the measurement of tissue T1 to monitor temperature in vivo by MRI. Magn Reson Med 1994; 31:342–345.
47. Matsumoto R, Oshio K, Jolesz FA. Monitoring of laser and freezing-induced ablation in the liver with T1-weighted MR imaging. J Magn Reson Imaging 1992; 2:555–562.
48. Cline HE, Hynynen K, Hardy CJ, Watkins RD, Schenk JF, Jolesz FA. MR temperature mapping of focussed ultrasound surgery. Magn Reson Med 1994; 31:628–636.
49. Alexander AL, Gmitro AF, Damianou C, Hynynen K, Ungar E. Optimization of gradient-echo pulse sequences for dynamic imaging of hyperthermia. In: Proceedings of the 2nd annual meeting of the Society of Magnetic Resonance. San Francisco: Society of Magnetic Resonance 1994; 1577.
50. Samulski TV, Macfall J, Zhang Y, Grant W, Charles C. Noninvasive thermometry using magnetic resonance diffusion imaging: potential for application in hyperthermic oncology. Int J Hyperthermia 1992; 8:819–829.
51. Zhang Y, Samulski TV, Joines WT, Mattiello J, Levin RL, Lebihan D. On the accuracy of noninvasive thermometry using molecular diffusion magnetic resonance imaging. Int J Hyperthermia 1992; 8:263–274.
52. Lebihan D, Delannoy J, Levin RL. Temperature mapping with MR imaging of molecular diffusion: application to hyperthermia. Radiology 1989; 171:853–857.
53. Niesman MR, Khoobehi B, Magin RL, Webb AG. Liposomes and diagnostic imaging: the potential to visualize both structure and function. J Liposome Research 1994; 4(2):741–768.
53a. Webb AG, Wong M, Wilmes LJ, et al. Use of liposome entrapped Co-59 complexes for non-invasive in-vivo temperature measurements. Int J Hyperthermia 1995; 11:821–827.
54. Franklin KJ, Buist RJ, den Hartog J, Mcrae GA, Spencer DP. Encapsulated liquid crystals as probes for remote thermometry. Int J Hyperthermia 1992; 8:253–262.